Elucidating ATP's Role as Solubilizer of Biomolecular Aggregate

Susmita Sarkar[1], Saurabh Gupta[2], Chiranjit Mahato[2], Dibyendu Das[2] and Jagannath Mondal[1]*

[1]Tata Institute of Fundamental Research Hyderabad, Telangana, India, 500046

[2]Indian Institute of Science Education and Research, Kolkata, Campus Rd, Mohanpur, Haringhata Farm, West Bengal 741246
email: jmondal@tifrh.res.in. Phone: +91-40-2020-3091

Abstract

Proteins occurring in significantly high concentrations in cellular environments (over 100 mg/mL) and functioning in crowded cytoplasm, often face the prodigious challenges of aggregation which are the pathological hallmark of aging and are critically responsible for a wide spectrum of rising human diseases. Here we combine a joint-venture of complementary wet-lab experiment and molecular simulation to discern the potential ability of adenosine triphosphate (ATP) as sollubilizer of protein aggregates. We show that ATP prevents both condensation of aggregation-prone intrinsically disordered protein Aβ40 and promotes dissolution of pre-formed aggregates. Computer simulation links ATP's sollubilizing role to its ability to modulate protein's structural plasticity by unwinding protein conformation. We show that ATP is positioned as a superior biological solubilizer of protein aggregates over traditional chemical hydrotropes, potentially holding promises in therapeutic interventions in protein-aggregation related diseases. Going beyond its conventional activity as energy currency, the amphiphilic nature of ATP enables its protein-specific interaction that would enhance ATP's efficiency in cellular processes.

Introduction:

Adenosine triphosphate (ATP), universally present in all living organisms, is recognized as a fundamental energy currency essential for a myriad of cellular processes. While its traditional role in energy metabolism is well-established, recent investigations have unveiled novel dimensions of ATP's involvement, specifically in protein stabilization and solubilization. Although the canonical functions of ATP are comprehensively understood, its impact on cellular protein homeostasis, particularly in the prevention of aggregation and the maintenance of membraneless organelles, remains a subject of growing interest[1–4].

Beyond its well-known chemical actions originating from high-energy phosphate bond breaking or allosteric effects during enzymatic catalysis, ATP exhibits contrasting physical biological roles,

including the stabilization of soluble proteins[5–7] and the solubilization of insoluble proteins[8–13]. Proteome-wide profiling analyses emphasize ATP-mediated protein stabilization as a prevalent trait within the ensemble of proteins featuring an ATP recognition site[2]. Subsequent independent studies further validate ATP-mediated enhancement of protein stability for specific proteins, such as ubiquitin, malate dehydrogenase[6], and the TDP-43 RRM domain[7], all possessing an ATP-binding motif. Intriguingly, these proteins, where ATP functions as a substrate or allosteric modulator, typically require a low concentration of ATP (approximately 500 μM) for its effects[2].

Notably, the cellular cytoplasm maintains a significantly higher concentration of ATP (~5mM), prompting questions about potential additional purpose for this elevated cytoplasmic ATP concentration beyond its conventional roles as an energy source and in protein stabilization, both typically requiring micromolar concentrations of ATP. As a potential function of the excess ATP concentration within the cell, a substantial influence on cellular protein homeostasis is observed, particularly in preventing protein aggregation [14–21] and maintaining the integrity of membraneless organelles (at a millimolar range of ATP concentration). ATP has demonstrated its capability to prevent the formation of protein aggregates, dissolve liquid-liquid phase-separated (LLPS) droplets, and disrupt pathogenic amyloid fibers[9].

Investigations into ATP's impact on protein solubility and aggregation encompass a diverse array of proteins, including phase-separating proteins like FUS, TAF15, hnRNPA3, and PGL-3[9], as well as the aggregates of Xenopus oocyte nucleoli[18]. Elevated ATP concentrations are also observed in metabolically quiescent organs, such as the eye lens, where they prevent the crowding of γS-Crystallin[16]. Proteome-wide profiling analyses underscore ATP's ability to manage the solubility of numerous proteins, indicating a broad impact on cellular protein solubility and aggregation propensity[2].

Remarkably, a majority of proteins lacking any ATP-binding motif, are reported to undergo solubilization in the presence of ATP. Despite past conformational analyses of water-soluble ATP-binding proteins in the presence of ATP[2], the role of ATP in biomolecular solubilization, specifically how ATP influences the structural plasticity of insoluble, non-ATP binding proteins, has yet to receive mainstream attention. In this investigation, we employ a combination of computer simulations and experimental techniques to explore how ATP influences the conformational behavior of two proteins situated at opposite ends of the structural spectrum of non-ATP binding proteins: the folded globular mini-protein Trp-cage and the amyloidogenic intrinsically disordered protein (IDP) Aβ40, associated with Alzheimer's disease (Figure 1). Our study, incorporating ThT assay and Transmission Electron Microscopy, validates hypotheses generated through computer simulations regarding ATP's

impact on the nucleating core of the Aβ40 peptide segment. The results establish a clear correlation between ATP's effect on the conformational landscape of these proteins and its ability to impede the aggregation process, affirming its role as a solubilizing agent.

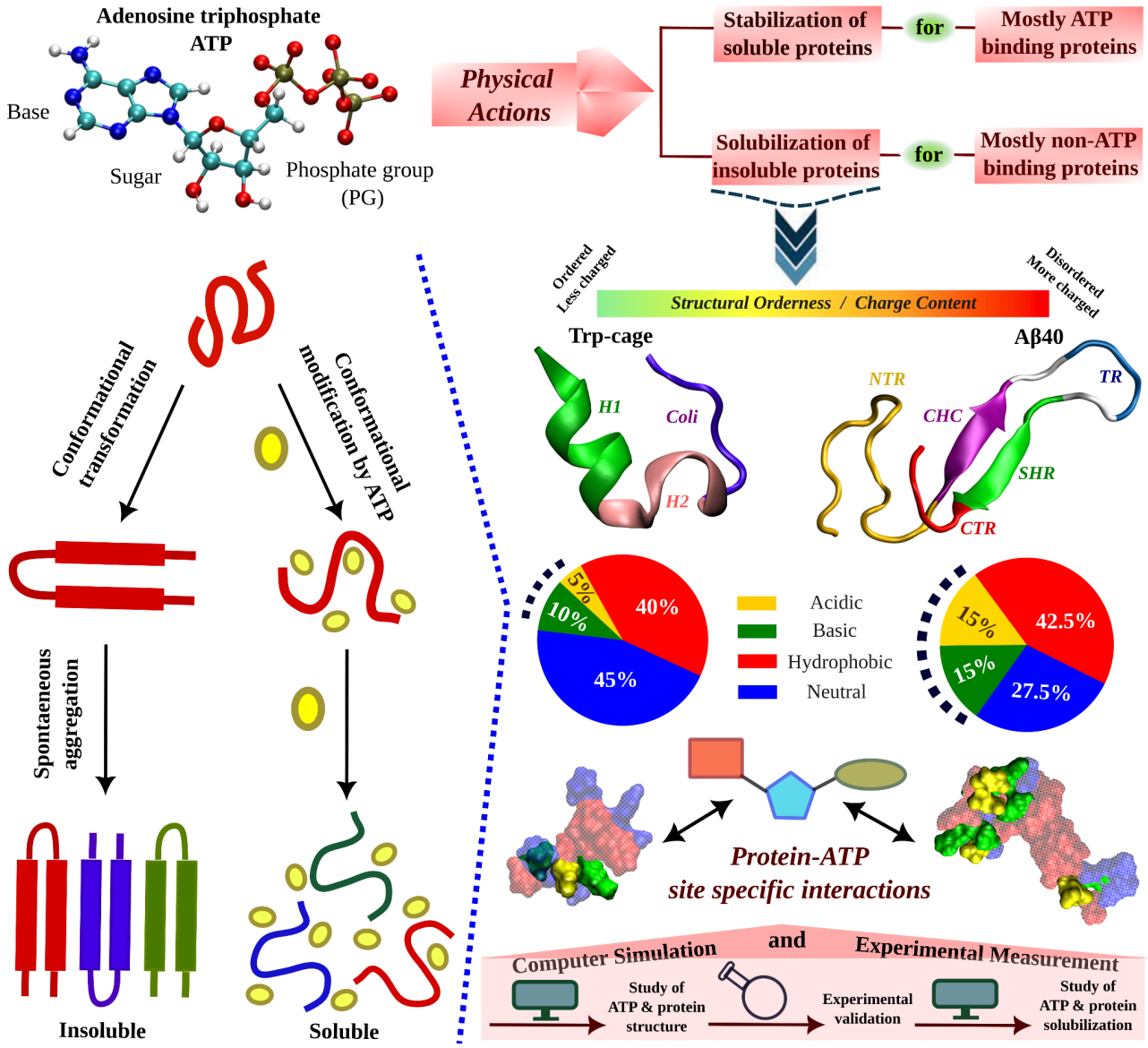

Figure 1: A schematic representation shows protein undergoes spontaneous aggregation in aqueous medium through specific conformational transformation prone to aggregation. ATP can prevent protein aggregation and improves its solubility. ATP's effect in protein conformational plasticity has been tested for two contrasting protein molecules belonging from two extreme spectrums of the protein family. One is the globular, structurally ordered protein Trp-cage and the other one is intrinsically disordered protein (IDP), Aβ40, containing comparatively more charged residues (according to the nature of typical IDPs). The highly aggregation prone Aβ40 protein is popularly well known for causing neurodegenerative disorders (*Alzheimer's disease, AD*). The structures of both the proteins are shown in the new cartoon representation highlighting the protein region wise coloration scheme. For Trp-cage the three distinct regions, 1. Helix (H1, 1-9), 2. 3-10 Helix (H2, 10-15) and 3. Coil (coil, 16-20) are shown in green, pink and navy blue colors respectively. For Aβ40, the 1. N-terminal region (NTR, 1-16), 2. central hydrophobic core (CHC, 17-21), 3. turn (TR, 24-27), 4. secondary hydrophobic region (SHR, 30-35), and the 5. C-terminal regions (CTR, 36-40) are shown in gold, purple, blue, green and red colors respectively. The hydrophobicity index of each of the proteins is shown in pie chart representation containing acidic (gold), basic (green), hydrophobic (red) and neutral (blue) residue content. Each of the proteins shown in the surface model are colored according to the respective hydrophobicity nature. Protein-ATP (base part: red, sugar

moiety: cyan and phosphate group: green) site specific interactions are tested. The current study of ATP's effect on protein conformational plasticity is performed combining both simulation and experiment based on computational predictions validated by experimental measurement followed by computational reasoning and correlation of ATP driven conformational modification to protein aggregation scenario.

Results and Discussion:

ATP's impact on a globular mini-protein: We initiated our investigation via computationally simulating ATP's effect on the archetypal monomeric form of mini-protein Trp-cage which is known to have a well-defined fold under native conditions (see Figure 1). The effects of ATP on the structure of the Trp-cage protein were investigated using classical molecular dynamics (MD) simulations. The protein was modeled with a99SB-*disp* forcefield and solvated with TIP4P-*disp* water molecules[22]. The system was neutralized with chloride ions. The protein was simulated in aqueous solution and also in presence of ATP, at a temperature of 303 K. The precedent experiments investigating protein aggregation in presence of ATP, had been performed by maintaining ATP:protein stoichiometric ratio in the range of $0.1x10^3$ to $1.6x10^3$. Likewise, in our simulation with Trp-cage, the ATP:protein ratio of $0.02x10^3$ was maintained.

Simulations were performed at three different concentrations of $ATP.Mg^{+2}$: 0 M (aqueous media), 0.1 M, and 0.5 M. For ensuring exhaustive exploration of protein conformational landscape condition, each condition was extensively simulated via replica exchange MD simulation (see method). The results showed that ATP caused the Trp-cage protein to unfold. This was evident from an increase in the protein's radius of gyration (R_g) and a decrease in the number of intra-chain contacts (see Figure 2 A-C). The R_g of the protein monotonically increased by the action of ATP compared to that of the neat water system in a concentration dependent manner (Figure 2A). The number of overall intra-chain contacts (Figure 2B) and native sub-set of intra-chain contacts (Figure 2C) monotonically decreased upon increasing the concentration of ATP from 0.1 M to 0.5 M. This is also evident from the inter-residue contact-map (see Figure S1 A-B). The two-dimensional free energy landscape of the Trp-cage protein was also calculated (see Figure 2 D-F). The landscape showed that the protein prefers to remain in its folded form (with less R_g and high native contacts) in the absence of ATP. However, in the presence of ATP, the landscape becomes more populated with conformations that have a higher R_g and fewer intra-chain contacts. This suggests that ATP drives the unfolding of the Trp-cage protein by stabilizing conformations that are more extended and disordered. The observation remains robust over the choice of force field. Similar to the results obtained with a99SB-*disp* forcefield, when the similar simulations were performed with Charmm36 force parameters of protein (with Charmm TIP3P water model) in 0 M and 0.5 M of ATP (modeled with Charmm36 force field parameters), the extension of the protein chain has been noted, as was characterized by the

stabilization of protein conformations with higher R_g and lower native contacts is attained in presence of ATP (figure S2). The event of unfolding of the protein upon addition of ATP is also evident from the simulation snapshots (see figure G-H). A comparative molecular analysis of secondary structure of Trp-cage in neat water versus ATP indicates reduction of both alpha-helical and 3-10 helical content (figure 3 A-B) along with inter-residue hydrogen bond (figure S3). Interestingly, the protein's solvent accessible surface area (SASA) increases slightly in presence of ATP (figure 3 C), implying that ATP can increase the solubility of protein, a point that we would later come back to.

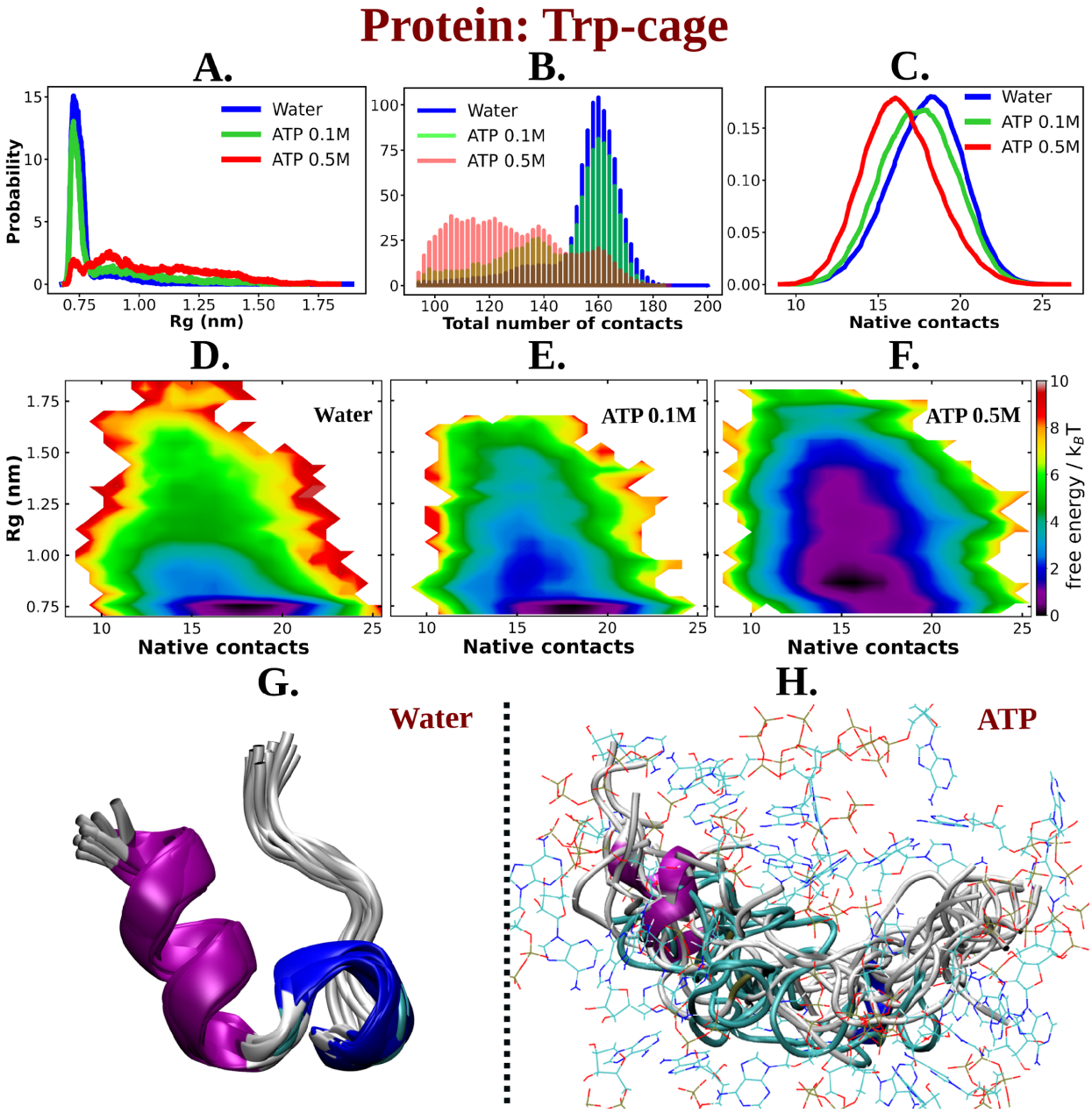

Figure 2: A. The probability distribution of R_g of Trp-cage compared in neat water and in 0.1 and 0.5 M ATP. B. Probability of the total number of contact formation among the residues of Trp-cage monomer are compared in absence (water) and presence of ATP (at 0.1 and 0.5 M). The probability distribution of native contacts (nc) of the protein in water and in 0.1 and 0.5 M ATP solutions are being shown in figure C. Figure D, E and F represent the 2D free energy profile of Trp-cage corresponding to the R_g and nc of the protein in water, 0.1 and 0.5 M ATP solutions respectively. Snapshots

containing overlay of protein's conformations in absence of ATP (neat water) and in presence of ATP (0.5 M) are shown in figure G and H respectively. Protein is colored by secondary structure and ATP molecules in figure H are shown in line representation with an atom based coloring scheme (C: cyan, N: blue, O: red).

The solvation shell of ATP around Trp-cage suggested its direct interaction with the protein (see figure 3 D for a snapshot). Analysis of the preferential interaction coefficient (Γ) profiles (see method for definition) provided insights into the relative influence of different chemical components of ATP (triphosphate group, sugar moiety, and aromatic base) on the protein (see figure 3 E). Consistently higher preferential interaction coefficient (Γ) profile of the aromatic base indicated that ATP's interaction with the protein is primarily driven by this moiety. This finding is supported by the hydrophobic nature of a significant fraction of Trp-cage residues (see Figure 1 for a pie chart of residue) and the predominance of van der Waals interactions in the favorable base part of ATP-protein interaction (figure 3 F). The preferential interaction analysis also revealed that the base part of ATP interacts more strongly with the helix (H1) region of Trp-cage compared to the 3-10 helix (H2) and coil structures (see figure 3 G). Consequently, the prominent interaction with the helical region results in a greater disruption of the helical structure (figure 3 H) compared to others (3-10 helical or coil), leading to improved solubilization potential. These results provide valuable insights into the specific interactions between ATP and protein as the key for ATP's actions and also enhance our understanding of the interplay between ATP and protein structure.

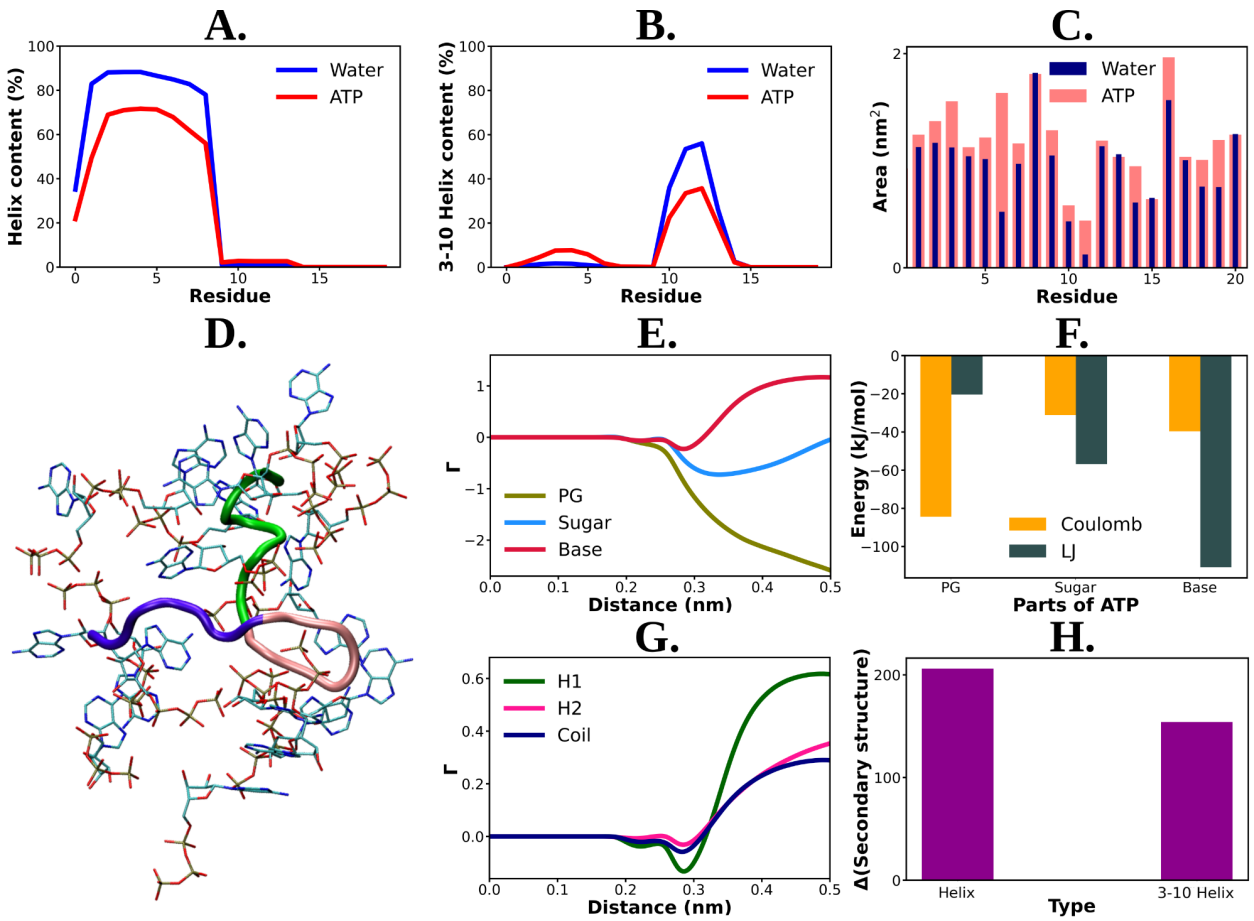

Figure 3: Residue wise total percentage of helix and 3-10 helix content of Trp-cage protein in absence and presence of ATP (0.5 M ATP) are shown in figure A and B respectively. Figure C. The solvent accessible surface area is calculated (with gromacs module of "gmx sasa") for Trp-cage and represented for the aqueous medium without and with ATP corresponding to each of the protein residues in a bar plot representation. Figure D shows a representative snapshot of ATP's (in licorice representation with atom based coloring scheme) interaction with Trp-cage (new cartoon representation. Green: H1 (1-9), pink: H2 (10-15), navy blue: coil (16-20)). E. Preferential interaction coefficient (Γ) of different parts of ATP: PG, sugar and base (with respect to solvent, water) with protein are being compared. F. Bar plot representation of coulombic and LJ interaction performed by all three different parts of ATP (PG, sugar and base) with Trp-cage. Figure G. represents the comparative plots of the preferential interaction coefficient (Γ) of ATP with the three structurally different parts (H1, H2 and coil) of Trp-cage. H. The change in the secondary structure content (helix and 3-10 helix) due to action of ATP are being represented. The difference in helix and 3-10 helix content in neat water from that of ATP solution are shown in bar plots.

ATP's impact on an Intrinsically Disordered Protein (IDP): The observation of ATP's unfolding effect on a model globular protein across a range of concentrations encouraged us to explore how its impact would vary on an IDP Aβ40, which sits at the other end of the spectrum of protein family. Aβ40 has also remained a regular subject of pathological neurodegeneration due to its self-aggregation propensity. Accordingly, extensively long MD (30 μs) simulation trajectory of monomeric Aβ40 in 50 mM aqueous NaCl media, as obtained from D. E. Shaw research, was analyzed[22]. To realize the effect of ATP on the conformational ensemble of Aβ40, we simulated the conformational repertoire of the monomeric form of Aβ40 in 0.5 M (ATP/protein stoichiometry

$0.1x10^3$) aqueous ATP solution containing 50 mM NaCl salt. The protein was modeled with CHARMM36m force field parameters and was solvated with TIP3P water molecules. To facilitate exhaustive sampling of Aβ40 in ATP medium, replica exchange MD (REMD) simulation was performed with a total 64 replicas in a temperature range of 290 to 460 K (see Method). A comparison of 2D free energy map (figure 4 A-B) along R_g and the total number of inter-residue contact of Aβ40 in aqueous media (later referred as water) containing no ATP and that in presence of 0.5 M aqueous ATP (later referred as ATP) indicates a clear shift of relative population of Aβ40 conformational sub-ensemble towards a basin with higher R_g and lower number of contacts in presence of ATP, suggesting unfolding of the protein chain by ATP. Representative snapshot of the conformation of Aβ40 in aqueous ATP media reveals significantly enhanced disorder in protein (figure 4 C). Aβ40 is also very prone to form β-sheet in aqueous medium and thus gets associated in extensive protein aggregation. The central hydrophobic core (residue 17-21), (CHC) [23] (shown in purple color in figure 1) participates in the β-sheet formation in water and acts as the nucleating core during the pathogenesis relevant to Alzheimer's disease (AD). Interestingly, as evident from the snapshots and from the relative comparison of ensemble-averaged residue-wise β-sheet propensity (figure 4 D), ATP reduces the content of β-sheet in CHC region and its partner β-fragment residue 30-35 (SHR, the secondary hydrophobic region). The decrease in the β-sheet signature in aqueous ATP solution is also apparent in the inter-residue contact map (figure 4 E-F).

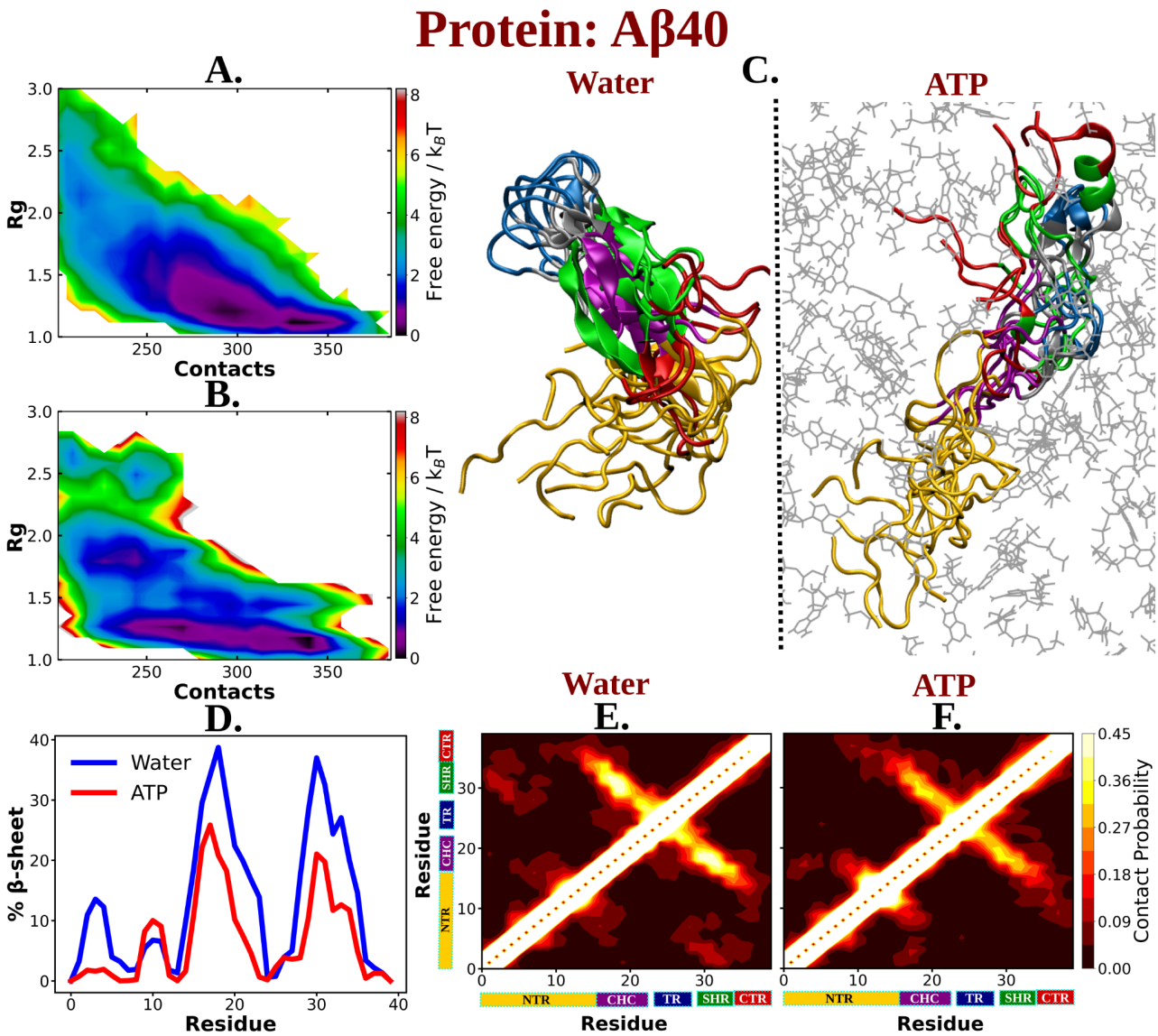

Figure 4: The 2D free energy profile of Aβ40 monomer estimated with respect to R_g and total number of intra-chain contacts are shown in figure A and B for Aβ40 in neat water and 0.5 M ATP respectively. Figure C. compares the simulation snapshots of Aβ40 monomer in neat water and in presence of ATP. Multiple conformations are overlaid for each of the cases to represent the statistical significance. Protein is colored region wise as done in Figure 1 and ATP molecules are shown by gray color line representation. Figure D. compares the β-sheet content of the Aβ40 protein in water and in 0.5 M ATP solution. Figure E and F show the residue wise intra chain contact map of Aβ40 in absence and in presence of ATP (0.5 M) respectively.

The presence of D23-K28 salt bridge [24–26] has been previously reported in the Aβ40 monomer present within aqueous medium. This salt bridge interaction subsequently gives rise to a structural motif which is sufficiently potent for nucleation. D23-K28 salt bridge interaction in Aβ40 has remained crucial in the context of fibrillogenic activities conducted by the pathogenic Aβ40. The salt-bridge interaction of D23-K28 stabilizes the β-turn[27] in the region of V24-N27[28,29] which consequently favors the hydrophobic contacts between the central hydrophobic core (CHC) and the C-terminal part of Aβ40. The structural bend in the zone of residue 23-28 through salt-bridge interaction helps the

CHC (residue 17-21) and SHR fragments (residue 30-35) to adopt β-sheet formation which gets further stabilized with L17-I32 hydrophobic interaction[30,31]. All these intramolecular interactions (salt-bridge interaction: D23-K28, β-turn: V24-N27, hydrophobic contact: L17-I32) within Aβ40 protein in water, effectively result in the adoption of the β-structure which might be critically responsible for its higher propensity to form pathological amyloid fibrils[32,33].

The present simulation trajectory of monomeric Aβ40 in 50 mM aqueous NaCl solution (water) traced all these aforementioned important fibrillogenic interactions. In particular in water the conformational ensemble of Aβ40 adopted D23-K28 salt-bridge, V24-N27 β-turn and L17-I32 hydrophobic interaction (figure 5 A-F), as evident from close pairwise distance of separation (see figure S4 A-C). These result in a constrained β-hairpin structure of Aβ40 in water which is capable of inducing aggregation. In presence of ATP (0.5 M ATP in 50 mM NaCl solution), contacts present in these motifs get significantly disfavoured (figure 5 A-F and S4 A-C), thereby substantially reducing the possibility of aggregation.

Interestingly, ATP's direct interaction (figure S5) with the protein molecule allows the disruption of all these pathogenic molecular interactions. Figure 5 G represents the ATP's region specific (PG, sugar and base) interaction with the protein Aβ40. The estimation of Coulombic and van der waal interaction energy indicates that unlike Trp-cage (figure 3 F), Coulombic interaction of ATP with protein predominates in Aβ40 (figure 5 H), partly due to higher proportion of charge in this IDP (see the pie chart for Aβ40 in figure 1). This result signifies that ATP works in the protein specific manner.

An analysis of solvation free energy of the protein (see method) in absence and in presence of ATP predicted that the presence of ATP in aqueous solution significantly decreases the free energy required to solvate the IDP (figure 5 I), hinting at the ATP's possible role in solubilizing the IDP. This was also evident in the ATP-induced increase in SASA of the protein (figure S6).

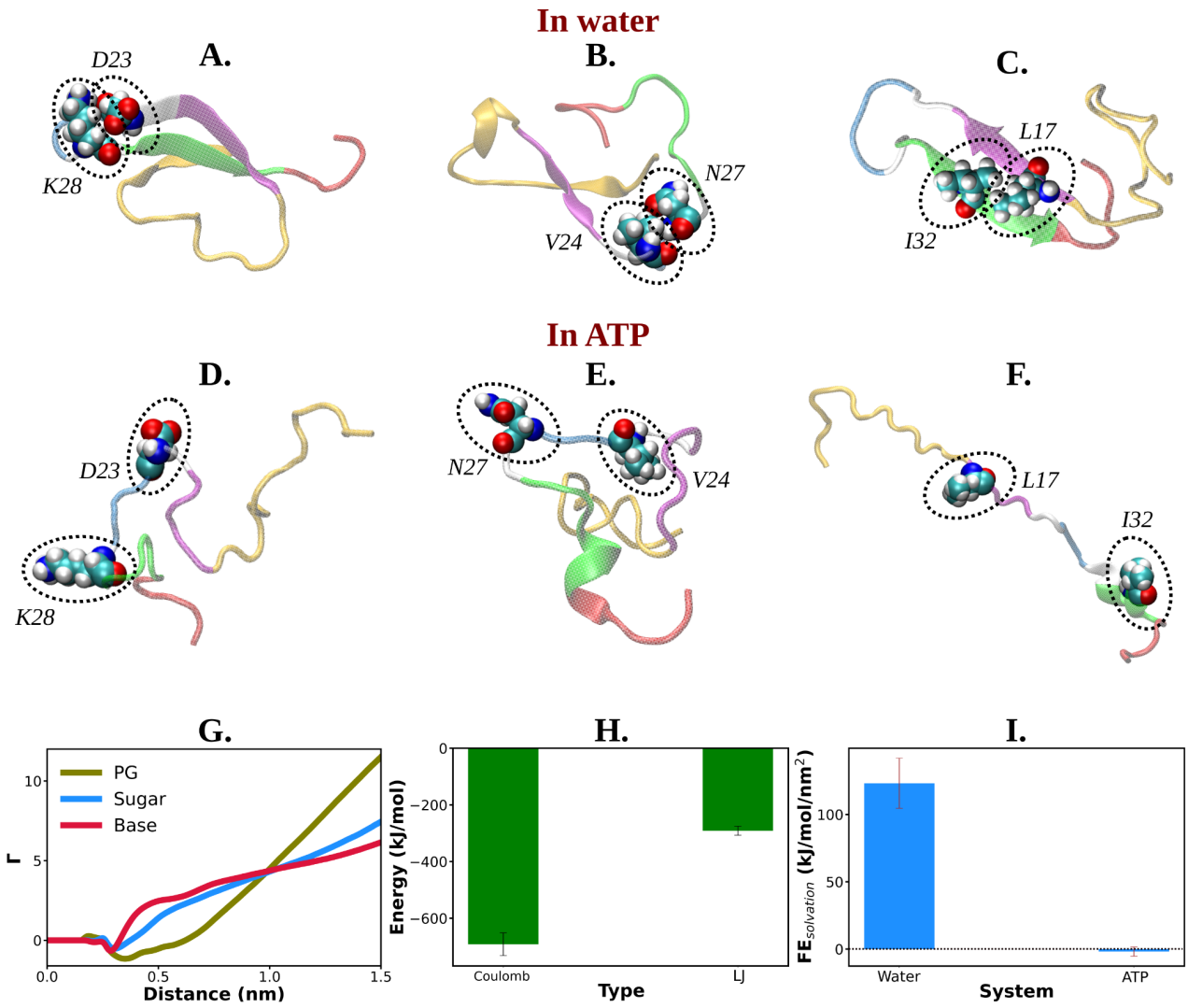

Figure 5: Figure A, B and C show the representative snapshots of different pairs of interacting residues namely, D23-K28, V24-N27 and L17-I32 respectively compared for salt water. The similar set of interactions are being represented in Figures D, E and F for ATP solution containing salt. G. Preferential interaction coefficient (Γ) of different parts of ATP (PG, sugar and base) with protein are being represented with respect to solvent water. H. The combined coulombic and LJ interaction energies imparted by all the three parts of ATP with Aβ40 are shown. I. The free energy of solvation (calculated by the gromacs module of "gmx sasa") of Aβ40 protein in absence and in presence of ATP are shown in a bar plot diagram. The vertical lines over the bars show the error bars.

Experimental Investigation of ATP's effect on aggregation of Nucleating core of Aβ40: The aforementioned computer simulation predicts that ATP has the potential to decrease the beta-sheet content within the nucleating core of monomeric Aβ40. This finding prompted us to conduct wet-lab experiments to investigate whether ATP plays a role in solubilizing the aggregation-prone Aβ content.

To explore experimental evidence of this influence on the dissolution of misfolded protein, we opted to focus on a shorter subset of the sequence rather than the entire sequence of the intrinsically disordered Aβ (1-40) amyloid. Consequently, we selected a short peptide stretch containing the important nucleating core of Aβ (1-40) from the 16th to the 22nd residue [Ac-KLVFFAE-NH_2, Ac-

KE] involving the fibrillogenic CHC region (figure 6 A)[34], which had been suggested by aforementioned computer simulation to impart crucial contribution in formation of β-sheet conformation. This nucleating core is potentially known to act as the intermolecular glue during aggregation. Lysine at the N-terminal and glutamic acid at the C-terminal facilitated an antiparallel arrangement during assembly formation, contributing to colloidal stability[35]. To initiate the assembly of Ac-KE, the synthesized peptide was dissolved in a solution consisting of 40% acetonitrile-water containing 0.1% trifluoroacetic acid (TFA, pH 2). Following an incubation period of approximately 11-15 days, the assemblies exhibited a characteristic β-sheet structure, as revealed by circular dichroism (CD), resembling that of Aβ amyloid (Figure S7)[36].

The impact of ATP on amyloid fibrils was investigated using the Thioflavin T (ThT) assay, a well-established method for probing amyloid assembly (Figure 6 B). In presence of Ac-KE assembly, ThT demonstrated an intense emission at 480 nm which suggested the presence of preformed amyloid aggregation (Figure 6 B)[37,38]. Various AcKE:ATP ratios, ranging from 1:0 to 1:66.7, were tested in HEPES buffer (pH 7.2, 10 mM) at room temperature to assess the influence of ATP on preformed amyloid assemblies (Ac-KE). Interestingly, a progressive reduction in ThT intensity at 480 nm in the presence of ATP (Figure 6C) was observed over time, compared to the control system, which contained only the peptide assembly (Ac-KE) in a similar environment (figure 6C). This decrease of ThT intensity in aqueous ATP solution reported the dissolution of the peptide assembly and disruption of the binding sites. Subsequently, morphological changes were examined using transmission electron microscopy (TEM) by casting the incubated samples on the TEM grid (see experimental measurement subsection in Method section). We expected that the investigation from electron microscopy would help in witnessing the visual transformation of fibrillar morphology in the presence of ATP. As a control experiment, the same concentration of Ac-KE assembly was also incubated without ATP in the similar environment for 18 h. Notably, micrographs recorded at different time frame supported the gradual dissolution of the peptide assembly when samples were incubated with ATP within 18 hours, while the control systems containing only Ac-KE did not demonstrate any noticeable alteration in their fibrillar morphologies (figure 7 A-C), library of TEM micrographs: figure S9-S11).

.

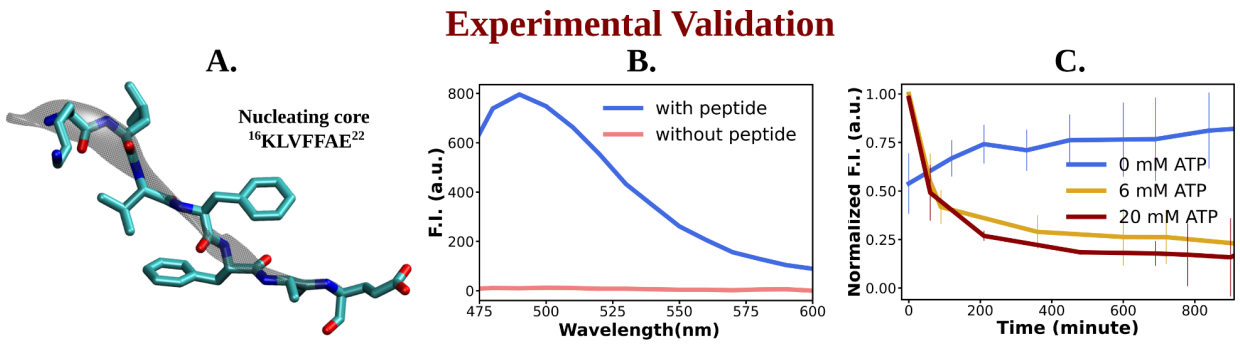

Figure 6: Figure A shows the representative snapshot of the peptide belonging to the nucleating core (16th to 22nd residue [Ac-KLVFFAE-NH_2, Ac-KE]) of the Aβ40 protein, which is utilized for the experimental measurements. Figure B represents emission spectra of ThT in the presence (blue) and absence (pink) of peptide assembly in 10 mM HEPES buffer pH 7.2. Excitation wavelength (λ_{ex}) = 440 nm. (Final concentration [Ac-KE]=200 μM, [ThT]=30 μM). Figure C shows a comparative plot of ThT (30 μM) assay of AcKE (300 μM) assembly with time in 10 mM pH 7.2 HEPES buffer with 0 mM (blue curve), 6 mM (yellow curve) and 20 mM (dark red curve) of ATP. The vertical lines over the bars show the error bars.

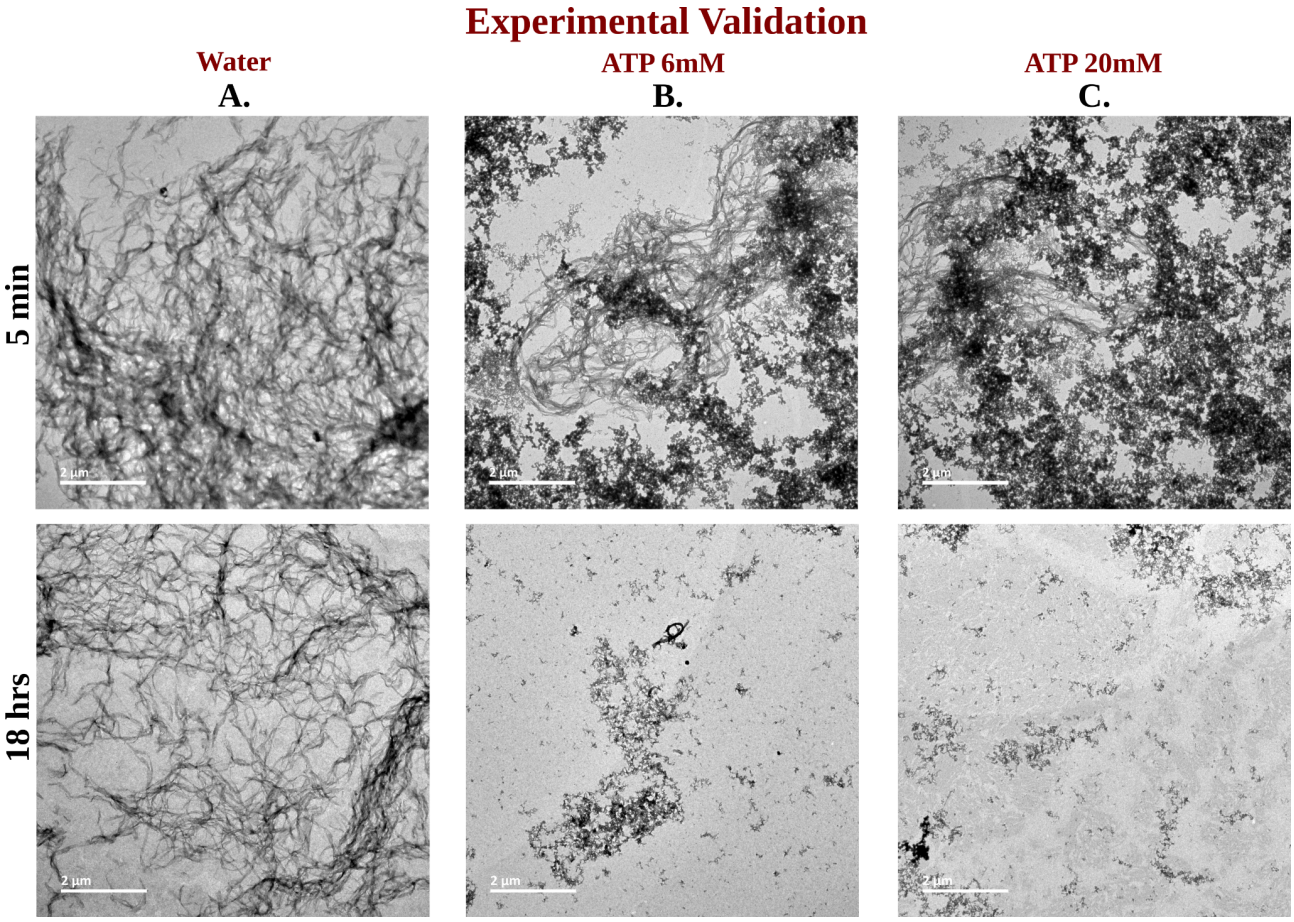

Figure 7: Library of TEM micrographs of Ac-KE (300 μM) assemblies in 10 mM pH 7.2 HEPES buffer at 5 min (up) and after 18 h (down) of incubation, in presence of A. 0 mM ATP B. 6 mM ATP and C. 20 mM ATP are being represented.

Molecular basis of ATP's solubilizing Role of Aβ40 aggregates: The experimental findings indicating ATP's potential role in solubilizing the fibrils of the Aβ40 nucleating core motivated us to

explore the molecular basis through the early step of oligomerization. To investigate this, we conducted computational simulations of the dimerization process of Aβ40 in aqueous ATP (0.5 M) media containing 50 mM NaCl and compared it with the same aqueous condition without ATP. Initially, three configurations were considered by placing two copies of the protein at a distance (see methods), and unrestrained molecular dynamics (MD) simulations were performed under both conditions, with and without ATP.

The time profiles of the distance between inter-protein contact pairs (involving CHC-CHC, figure 8A, and involving CHC-SHR, figure 8B) revealed that, within the simulation time frame, the pair of Aβ40 approached each other and formed a dimer. However, the propensity for Aβ40 dimerization was significantly diminished in aqueous ATP media. The residue-wise inter-protein contact map of Aβ40 in the absence and presence of ATP molecules (figure 8 C-D) further illustrated the disappearance of multiple contact densities in the presence of ATP. Contacts such as CHC-CHC, CHC-SHR, and SHR-SHR[39], which were highly likely to form between protein pairs in aqueous saline medium, did not appear at all in the presence of ATP (figure 8 D).

The nucleating core (involving the CHC region) of Aβ40, the same motif used in the previously described wet-lab experiment, played a crucial role as an intermolecular glue. Its active involvement in strong interactions with neighboring Aβ40 protein chains hindered the onset of protein aggregation via the first step of dimerization.

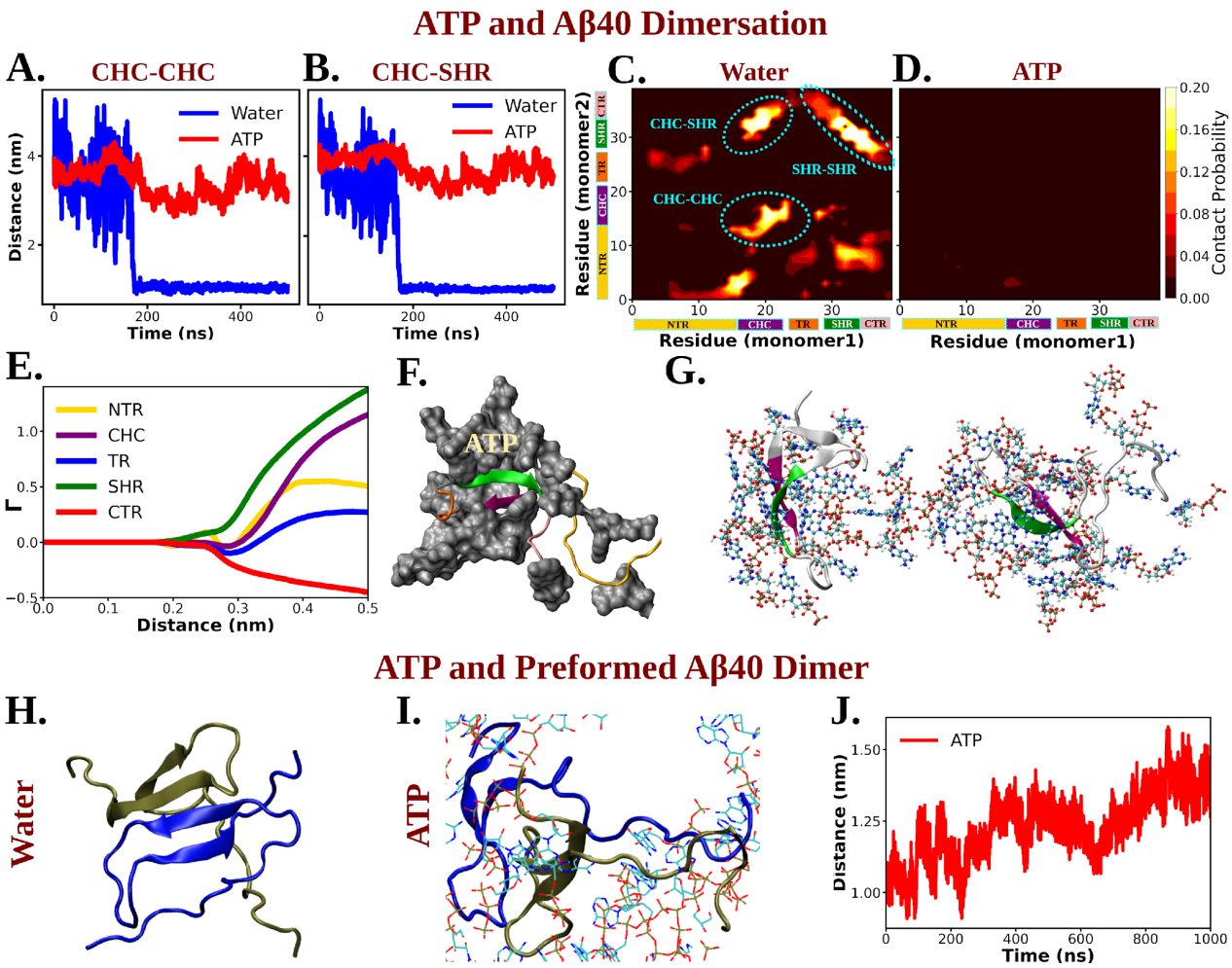

Figure 8: Figure A and B show the time profile of distance between the two actively interacting regions of two protein chains namely CHC-CHC and CHC-SHR respectively both in neat water and in presence of ATP co-solute (0.5 M ATP in 50 mM NaCl solution). Figure C and D represent residue-wise inter-protein contact map of Aβ40 in water and in 0.5 M ATP solution respectively. The contacts (CHC-CHC, CHC-SHR, SHR-SHR) found in neat water are highlighted. Figure E. The preferential interaction coefficient (Γ) of ATP with each different part of Aβ40 protein (NTR, CHC, TR, SHR and CTR) are being shown. F. Interaction of Aβ40 protein chain with ATP cosolute. ATP molecules are being shown in vdw representation. G. The interacting ATP molecules crowd around the two Aβ40 protein chains are being shown. Figure H and I show the consequence of Aβ40 dimer in neat water and in presence of ATP respectively. The corresponding simulation snapshots are being shown for simulation starting with Aβ40 dimer in water and in 0.5 M ATP in 50 mM NaCl solution. Figure J represents the time profile of distance between the two protein copies of the preformed Aβ40 dimer in exposure to ATP solution (0.5 M ATP in 50 mM NaCl solution).

The direct interaction of ATP with Aβ40, playing a pivotal role in attenuating protein-protein interactions, is evident from the preferential interaction coefficient (Γ) of ATP (figure 8E) with different parts of Aβ40 (NTR, CHC, TR, SHR, and CTR). Notably, ATP exhibits the strongest interactions with CHC and SHR (followed by NTR, TR, and CTR). These regions, as highlighted in the inter-residue contact map in the absence of ATP (Figure 8C), predominantly participate in inter-protein interactions during Aβ40 dimerization (refer to figure 8F for a snapshot). A representative

snapshot (figure 8G) illustrates the effective crowding of ATP molecules around Aβ40, preventing protein copies from engaging in intermolecular interactions.

The preferential interaction of ATP can also help to lower the probability of intermolecular steric zipper type interaction (M35-M35)[40] which plays a crucial role in aggregation. The inter-chain M35-M35 involving steric zipper interaction is important in forming amyloid fibrils by stabilizing sheet-to-sheet packing with the non-polar zipper. ATP can disrupt the steric-zipper interaction through its direct interaction (figure S8 A) with M35 residue Aβ40 as ATP makes it less available for intermolecular interaction through crowding (figure S8 B).

ATP's solubilizing ability of preformed oligomers: ATP not only prevents protein aggregation but can also dissolve pre-existing protein droplets, effectively maintaining proteostasis within cells. To explore ATP's action on a preformed dimer, simulations were initiated with the already-formed protein dimer conformation and simulated its fate in a 50 mM NaCl solution, both with and without the presence of 0.5 M ATP in the same saline medium (figure 8H-J). Interestingly, ATP was found to disrupt the dimer structure (figure 8I), while the structure remained stable in the absence of ATP (figure 8H). As characterized by the time-profile of the distance, the two protein chains (figure 8J), which were initially part of the dimer, gradually moved away from each other due to the action of ATP. This demonstrates that, in addition to inhibiting the formation of new protein aggregates, ATP is potent enough to disassemble existing protein droplets, maintaining proper cellular homeostasis. In summary, ATP has been observed to prevent protein condensation, dissolve previously formed condensates, and thereby enhance the solubility of biomolecules within aqueous cellular environments for proper cellular functions.

Is ATP special in its role as an aggregate solubilizer ? A crucial question rises: Is ATP special in its role as an aggregate solubilizer ? Towards this end, to investigate ATP's relative efficiency in inducing the solubility of hydrophobic entities (biological macromolecules) within cells, we compared it to a conventional chemical hydrotrope sodium xylene sulfonate (NaXS), routinely used in various industrial applications to solubilize sparingly soluble compounds in water. Simulations were conducted with two copies of Aβ40 proteins in a 0.5 M NaXS solution, similar to those performed for 0.5 M ATP and 0 M ATP scenarios (discussed earlier; see methods for details).

Figure 9A illustrates the time profile of the distance between two protein monomers in 0.5 M NaXS solution compared with that in ATP solution (0.5 M) and neat water. Interestingly, ATP prevents the protein chains from coming closer to each other, while in NaXS solution, the proteins exhibit comparatively closer proximity. This trend is further emphasized by the probability distribution of

the interprotein distance (figure 9B), which shows a gradual decrease in the distance between protein chains from neat water to 0.5 M NaXS solution and finally to 0.5 M ATP. This suggests that, compared to NaXS, ATP is more efficient in enhancing solubility in aqueous medium by preventing the formation of aggregates.

For a quantitative assessment of ATP's efficiency over NaXS, we calculated the bound percentage of protein monomers in each of the three cases (figure 9C). NaXS in water reduces the percentage of bound slightly, indicating a decrease in protein aggregation. However, ATP outperforms NaXS by significantly reducing the propensity of Aβ40 dimerization.

The potency of ATP in inhibiting protein aggregation and maintaining solubility in an aqueous environment, compared to NaXS, is further evident from the estimation of the total number of interprotein contacts (figure 9D). As we move from neat water to 0.5 M NaXS solution and finally to 0.5 M ATP solution, the number of intermolecular contacts between the two protein chains gradually decreases, highlighting ATP's efficiency over NaXS.

The contact map (residue-wise inter protein contact map) difference (contact map of ATP/NaXS+water from that in neat water only) reveals that in the presence of ATP, there is a significant decrease in the probability of interprotein contacts (figure 9E), a crucial factor in protein aggregation (figure 8C). In contrast, in the presence of NaXS (figure 9F), along with a decrease in some contact probabilities, there is an increase in interprotein contacts, especially involving the CHC and TR region of one chain with the SHR region of the other protein.

In nutshell, ATP acts more efficiently compared to NaXS by effectively inhibiting interprotein interactions, preventing aggregation, and maintaining protein solubility in an aqueous environment (figure 9G-H). To elucidate the factors contributing to ATP's superiority over NaXS, we examined the interaction energy of both ATP and NaXS with the protein molecules (figure 9I). The analysis revealed that, in comparison to NaXS, ATP exhibits a stronger interaction with the proteins, resulting in higher interaction energy. This heightened interaction energy plays a crucial role in preventing protein-protein interactions, ultimately leading to the effective inhibition of aggregation.

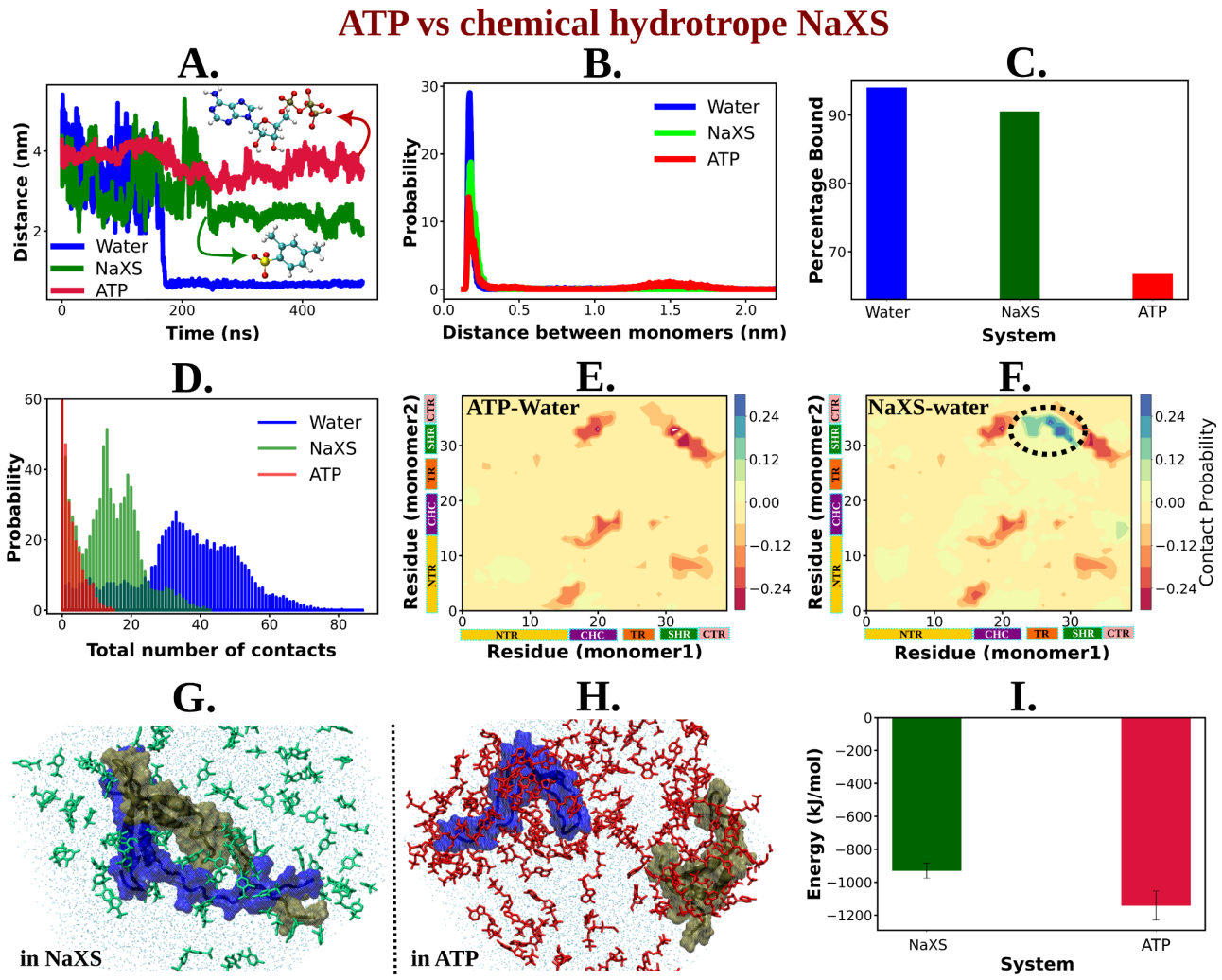

Figure 9: Figure A shows the time profile of distance between the two protein chains (CHC-CHC) in neat water (blue curve), in 0.5 M NaXS (green curve) and ATP (red curve) in 50 mM NaCl solution. Figure B represents the probability distribution of the distance between the protein chains in each of the three (above mentioned) cases. Figure C shows the percentage of bound of the proteins (for all the three systems) in a bar plot representation. Figure D depicts the total number of intermolecular contacts of the protein monomers in each of the three solutions. Figure E and F represent the difference of residue-wise inter-protein contact map of Aβ40 in 0.5 M ATP and 0.5 M NaXS solution respectively from that of the neat water system. Figure G and H show the representative snapshots captured during the Aβ40 dimerization simulation in 0.5 M NaXS and 0.5 M ATP solution respectively. Figure I represents the interaction energy between the NaXS (green bar) and ATP (red bar) molecules with the protein molecules in a bar plot representation. The vertical lines (black colored) show the error bars in the estimation.

Discussion and Conclusion:

While previous efforts have explored ATP-driven protein disaggregation, its impact on protein conformational plasticity, crucial for self-assembly, is understudied. Our computational investigation prioritizes the examination of ATP's influence on protein conformational thermodynamics and correlates it with preventing protein aggregation. Regardless of biomolecular structure (globular or intrinsically disordered), ATP is found to induce protein chain extension, disrupting specific secondary structures and promoting flexibility for solvation in water. We demonstrate ATP's direct

enhancement of protein aqueous solubility through calculations of solvation free energy and solvent-accessible surface area (SASA). The substantial increase in accessible surface area and more negative solvation free energy in aqueous ATP solution compared to ATP-free solution highlights ATP's pivotal role in preventing protein aggregation by increasing aqueous solubility through protein chain extension.

We followed up the simulation's prediction on ATP's role on protein conformation via a set of proof-of-concept experiments, in which we investigated ATP's impact on the fibrillogenic nucleating core of Aβ40 (residues 16th to 22nd). ThT assays revealed a monotonically decreasing intensity over time with increasing ATP concentrations (0 mM to 20 mM), indicating the dissolution of Aβ40 peptide assemblies. Transmission electron microscopy (TEM) confirmed the dissolution of peptide assemblies within 18 hours in ATP-treated samples, contrasting with control systems containing only Ac-KE, which showed no significant alteration in fibrillar morphologies. This experimental evidence, coupled with insights into ATP's role in enhancing aqueous solubility, necessitates an understanding of its molecular inhibitory mechanisms at the oligomerization level.

Computational studies focused on the primitive aggregation stage, specifically Aβ40 dimerization, revealed that ATP disrupts dimer formation compared to the rapid dimerization observed in water. ATP's ability to guide conformational changes, particularly by disfavoring β-sheet adoption between the CHC and SHR fragments, efficiently inhibits Aβ40 dimerization. Direct interactions between ATP molecules and the protein were identified as crucial, preventing pathological interactions (CHC-CHC, CHC-SHR, SHR-SHR) associated with the β-sheet motif. Additionally, ATP not only inhibits aggregation but also disintegrates previously formed dimers, highlighting its capability to dissolve existing protein aggregates. Overall, ATP's multifaceted action, from inhibiting dimerization to disrupting existing dimers, underscores its potential in preventing pathological protein aggregation.

In conclusion, beyond its role in various energetic modulations, ATP contributes significantly and independently of energy expenditure to the proper functioning of proteins in crowded cellular environments with high salt concentrations, mitigating biomolecular instabilities linked to diseases involving pathological protein aggregation. Our study demonstrates that ATP's micromanagement starts at the protein monomeric level, orchestrating conformational modifications to ensure adequate aqueous solubility. By perturbing intramolecular contacts, ATP induces structural flexibility, facilitating effective water solubilization of protein monomers. Simultaneously, ATP discourages the adoption of fibrillogenic protein conformations prone to aggregation. Recently described as hydrotropic activity, our findings provide a detailed understanding of the biological rationale for the

exceptionally high concentration of ATP in cells compared to other nucleotides, as reported by Patel et al. (2017)[9]. While previous studies highlighted ATP's antiaggregation property, our investigation elucidates its mechanism: ATP's remarkable influence on protein conformational modification helps hydrophobic protein molecules remain favorably soluble in the cellular aqueous medium, thereby reducing their propensity for self-aggregation. Overall, ATP's regulatory role in conformational plasticity emerges as a key factor behind its hydrotropic function in biological systems.

The mechanistic details of ATP's interaction with proteins have been subjected to various interpretations. Few studies proposed a nonspecific ATP-protein interaction[41,42], contrasting with the some reports explaining ATP's preferential binding to conserved residues (Arg and Lys)[43,44]. Some studies highlighted ATP's role as a solvation mediator with the capabilities of ATP in hydrophobic, π-π, π-cation, and electrostatic interactions with proteins[45–48]. In our investigation, we found that ATP interacts directly with Trp-cage and Aβ40 proteins in a protein-specific manner, utilizing its chemically distinct parts—negatively charged PG group, hydrophilic sugar moiety, and hydrophobic aromatic base—to engage in electrostatic, H-bond-like, and hydrophobic interactions with protein residues. The nature of ATP's interactions varies significantly based on the amino-acid composition of the protein. For the hydrophobic Trp-cage, ATP favors van der Waals' interactions over electrostatic ones, while for the charged Aβ40, Coulombic interactions dominate. This protein-dependent specificity enhances ATP's efficiency in cellular processes, aligning with recent proteome-wide[49] studies showing diverse effects of ATP on protein thermal stability and solubility. Notably, intrinsically disordered proteins experience enhanced solubility with ATP, while some proteins exhibit decreased solubility.

In our literature survey of ATP's concentration-dependent actions, as detailed in the Introduction section, we observed a dual role where ATP induces protein liquid-liquid phase separation at lower concentrations and promotes protein disaggregation at higher concentrations[50–52]. These versatile functions emphasize ATP's pivotal role in maintaining a delicate balance between protein stability (at low ATP concentrations) and solubility (at high ATP concentrations) for effective proteostasis within cells. Notably, ATP-mediated stabilization primarily targets soluble proteins, particularly those with ATP-binding motifs, while ATP-driven biomolecular solubilization is observed for insoluble proteins, typically lacking ATP-binding motifs. The question arises: how does ATP selectively stabilize or destabilize proteins? Recent proteome-based[53] investigations align with previous study[54] indicating that ATP predominantly stabilizes soluble bio-molecules, especially those featuring the P-loop motif (GK[X]nS/T or G[X]nK[X]nK). Our Sequence-based analysis of reported proteins, including ubiquitin, malate dehydrogenase, and TDP-43 RRM domain, reveals conservation of the

P-loop motif in their respective ATP-recognition site (see SI). Conversely, proteins like Trp-cage and Aβ40, undergoing ATP-driven solubilization at the expense of conformational stability, lack the P-loop motif (see SI). This suggests that ATP deciphers information from the primary structure (protein sequence) to govern secondary and tertiary structures, selectively stabilizing ATP-binding proteins and inducing solubilization in the absence of ATP-binding motifs during protein unfolding.

In summary, the distinctive protein-dependent and region-specific interactions between ATP and protein molecules play a pivotal role in regulating protein structure. This interaction mechanism leads to an exceptionally efficient inhibition of protein aggregation compared to conventional chemical hydrotropes. ATP orchestrates a two-stage hydrotropic action, from monomer destabilization to early-stage aggregation prevention. The necessity for higher cellular concentrations of ATP underscores its significance, potentially explaining the frequent onset of protein aggregation-related diseases with aging, attributed to ATP deficiency. The collaborative efforts of simulation and experimentation in this study suggest potential implications and therapeutic interventions using ATP for future treatments of various neurodegenerative diseases.

Method and Materials:

A. Simulation model and methods:

In this work, we have studied the effect of ATP on the conformational plasticity of two different types of proteins belonging from the contrasting protein spectrum: 1. folded globular protein, Trp-cage which stands as one of the very suitable prototypical computational mini-protein models with less charge content and 2. the intrinsically disordered protein, Aβ40 containing higher proportion charged residues (in line with the typical nature of IDP), which is popularly known for its characteristic high aggregation propensity (Figure 1). Here we have individually investigated the conformational dynamics of both the proteins in absence and presence of ATP-Mg^{2+}. The folded protein Trp-cage, PDB: 1L2Y, (both the N and C terminal of the protein was capped with acetyl group and methyl amide respectively) was studied in neat water and in 0.1 M and 0.5 M aqueous ATP solution (protein/ATP stoichiometry of 0.02×10^3). Further equivalent number of Mg^{2+} ions were incorporated into the simulation box. The system was charge neutralized with an equivalent number of chloride ions. The protein was modeled with a99SB-*disp* forcefield parameters and solvated with TIP4P-*disp* water molecules[55]. The ion parameters were taken from a99SB-*disp* forcefield. During simulation with ATP-Mg^{2+} (0.1 M and 0.5 M), ATP molecules were modeled with Amber force field parameters. For Trp-cage simulations in neat water and 0.5 M ATP-Mg^{2+} aqueous solution the box volume was

4.4x4.4x3.1 nm^3 and for 0.1 M ATP-Mg^{2+} simulation with Trp-cage the box dimension was kept fixed as 8.2x8.2x5.7 nm^3.

First each system was energy-minimized followed by two consecutive steps of equilibration: 1. NVT equilibration for 1 ns at an equilibrium temperature of 300 K utilizing the Nosé–Hoover thermostat[5657] (1 ps time constant) and then 2. equilibration in NPT ensemble for 2 ns at 300 K temperature and 1 bar pressure maintained using the Nosé–Hoover thermostat (time constant of 1 ps) and Berendsen barostat[58] (time constant of 1.0 ps) respectively. Further the system was again equilibrated in the NPT ensemble for 10 ns at an equilibrium temperature of 300 K and an equilibrium pressure of 1 bar, maintained by employing the Nosé–Hoover thermostat (time constant of 1 ps) and the Parrinello–Rahman barostat[59] (time constant of 1.0 ps) respectively. The particle-mesh Ewald (PME)[60,61] method with a grid spacing of 0.12 nm was applied for managing long-range electrostatics. For constraining the bonds associated with hydrogen atoms and the bonds and angle of water molecules, the LINCS method[62] and SETTLE algorithm[63,64] respectively were used. To perform all the molecular dynamics (MD) simulations GROMACS[65] software of version 20xx software was utilized.

To ensure exhaustive exploration of protein conformational landscape conditions, each condition (Trp-cage in neat water and 0.1 M and 0.5 M ATP-Mg^{2+} aqueous solution of Trp-cage) was simulated via Replica exchange molecular dynamics (REMD) simulation[66]. For performing REMD simulation the former equilibrated systems were employed. REMD simulation was done in the temperature range of 280–540 K with a total of 54 replicas (for 0.1 M ATP-Mg^{2+} solution the temperature range was 290-460 K with 64 replicas). At first each of the replicas was well equilibrated for 5 ns in the NVT ensemble at the respective replica temperature employing the Nosé–Hoover thermostat (time constant 1 ps). Eventually the production simulations were performed for 400 ns (250 ns for 0.1 M ATP-Mg^{2+} solution of Trp-cage) at each replica with a replica exchange interval of 10 ps. Finally the trajectory corresponding to the replica temperature of 303 K was considered for subsequent analysis. Further to test the robustness of our estimation across the choice of force field, the similar set of simulations for the Trp-cage protein in neat water and in 0.5 M ATP are performed with Charmm 36 force field parameters for protein[67] and ATP[68] and using Charmm TIP3P water model[69,70]. For these simulations in the Charmm36 force field the similar simulation protocol has been utilized.

Apart from folded globular protein, for studying ATP's effect on the conformation plasticity of an intrinsically disordered protein we have chosen Aβ40 which is routinely investigated in the context of protein aggregation related pathogenic conditions. Accordingly, the 30 us long MD simulation trajectory of monomeric Aβ40 in 50 mM aqueous NaCl media, from D. E. Shaw research was utilized[71]. To realize the impact of ATP on the conformational dynamics of Aβ40, we simulated the

conformational repotiare of monomeric form of Aβ40 in 0.5 M (ATP/protein stoichiometry $0.1x10^3$) aqueous ATP solution containing 50 mM NaCl salt. At first the protein was incorporated in the simulation box of dimension 8.2x8.2x5.7 nm^3 followed by addition of ATP molecules to maintain ATP concentration of 0.5 M. Equivalent numbers of Mg^{2+} ions were added. Finally the system was solvated with water molecules sufficient to fill up the box. The protein was modeled with charmm36m force field parameters[72] and for water molecules, Charmm TIP3P water model was employed[73,74]. The ion parameters are obtained from the Charmm 36m forcefield. ATP molecule is modeled with Charmm36 force field parameters[75]. For exhaustive sampling of the protein in ATP medium, replica exchange MD simulation was performed with a total 64 replicas in a temperature range of 290 to 460 K. Each of the replicas were simulated for 400 ns at the replica exchange interval of 10 ps, leading to a cumulative sampling aggregate equivalent to around 26 microseconds. The REMD conformations corresponding to 303 K were further clustered into 213 clusters via the R_g and total number of inter-residue contacts of the protein chain based on regular space clustering algorithm. Finally, 213 independent MD simulations were performed for 100 ns (each) with the different initial configurations (Aβ monomer dissolved in 0.5 M ATP in 50 mM aqueous NaCl solution) chosen randomly from individual clusters. The concatenated short trajectories were employed for generating 2D energy profiles and for all other calculation 303 K REMD simulation trajectory was employed. The 213 short MD simulation trajectories are used separately for building a Markov state model (MSM)[76] in order to statistically map the complete process of protein conformational change using PyEMMA software[77,78]. From MSM, the stationary populations of the discrete microstates were calculated and eventually utilized for reweighing the free energy surfaces obtained from these short trajectories.

Further to test the correlation of ATP's effect on protein monomeric level with its potency to inhibit aggregation, we have carried out equilibrium dimer simulations with the aggregation prone amyloidogenic protein aβ40. We have started our simulation from three different conformations involving the protein chains at three different distances 1 nm, 2 nm and 4 nm. Two replica simulations are performed with each of the configurations for 500 ns following the similar simulation protocol as mentioned above. The similar set of dimer simulations were performed for the two copies of the Aβ40 proteins in the 50 mM aqueous NaCl solution and also 0.5 M aqueous ATP solution containing 50 mM NaCl salt. The same box size was maintained for each of the dimer simulations as 8.2x8.2x5.7 nm^3 (same as the monomeric Aβ40 simulation with ATP-Mg^{2+}). Later we have repeated the similar dimer simulations for 0.5 M NaXS in the 50 mM aqueous NaCl solution, following the similar simulation protocol.

To assess the impact of ATP on the pre-existing protein droplets, we have tested ATP's effect on the preformed dimer. We have started our simulation with preformed Aβ40 dimer (three dimer conformations were obtained from the previously described Aβ40 dimerization simulation in 50 mM NaCl salt solution and simulations were carried out corresponding to each of the dimer conformation) dissolved in 0.5 M ATP-Mg^{2+} in 50 mM aqueous NaCl solution. Simulation was performed in the same box size of 8.2x8.2x5.7 nm^3 following the similar simulation protocol. Simulation was continued up to 1 us.

GROMACS software analysis tools were utilized for computing the radius of gyration (R_g), number of hydrogen bonds of the proteins. The fraction of native contacts (for Trp-cage) was estimated using PLUMED software[79] with a cutoff of 0.7 nm. For calculating the total number of contacts and residue-wise contact map MDAnalysis[80] tool was employed along with python scripting. The secondary structure content of each of the proteins was estimated using the STRIDE program of VMD. The calculation of the solvent accessible surface area was performed with the help of the GROMACS analysis tool (gmx sasa). The 2D free energy profiles were computed for each of the systems using the PyEMMA tool. The hydrophobicity index of each of the proteins was obtained from the peptide 2.0 web server "https://www.peptide2.com/N_peptide_hydrophobicity_hydrophilicity.php". For quantitative estimation of ATP's interaction with the proteins, the Wyman–Tanford preferential interaction coefficient[81,82] (Γ_s) was calculated with respect to water.

$$\Gamma_s = \left\langle n_s - \frac{N_s^{tot} - n_s}{N_w^{tot} - n_w} \cdot n_w \right\rangle$$

where n_s is the number of cosolute bound with the protein molecule and N_s^{tot} is the total number of the species present within the system. n_w represents the number of water molecules bound to the surface of the protein and N_w^{tot} is the total number of water of the system.

B. Experimental Measurements:

Materials:

All protected amino acids, activator N,N' Diisopropylcarbodiimide (DIC), N,N-diisopropylethylamine (DIPEA), Trifluoroacetic acid (TFA), piperidine, Uranyl acetate, Thioflavin T and HEPES were purchased from Sigma Aldrich. Oxyma was purchased from Nova Biochem. All

solvents and Fmoc-Rink amide MBHA Resin were purchased from Merck. Milli-Q water was used throughout the experiments.

Peptide Synthesis and Characterization

Ac-KLVFFAE-NH_2 (Ac-KE) peptide was synthesized by solid phase peptide synthesizer (CEM Liberty Blue). Fmoc-Rink Amide MBHA resin (loading 0.52 mmol/g) was swollen using dimethylformamide (DMF) for 15 min, followed by Fmoc deprotection with 20% piperidine in DMF. Each Fmoc-amino acid coupling step was performed using DIC and oxyma pure in DMF. Subsequently, acetylation of the N-terminus lysine was done using acetic anhydride in DMF. The resin was washed with dichloromethane (DCM) after completion of the final coupling and allowed to dry in open air. Peptide was cleaved from the resin using TFA/triethyl silane (5:0.1 v/v) solution for 2 h, followed by precipitation in cold diethyl ether after removing the TFA. The product was centrifuged at 5000 rpm for 15 min at 4 °C in Eppendorf centrifuge 5804 R and further, the pellet was washed 3 times with cold diethyl ether. Molecular mass was confirmed by Waters Xevo G2-XS QTof.

Ac-KLVFFAE-NH_2 (Ac-KE) ($C_{45}H_{67}N_9O_{10}$) (m/z) calculated for [$M+H^+$]: 894.50; found: 894.52

Peptide assembly

The dried powder of the peptide (Ac-KLVFFAE-NH_2) was treated with HFIP to eliminate preformed assembly during precipitation in ether. After that, HFIP was removed through N_2 blowing and the peptide film was dissolved in 40 % acetonitrile-water containing 0.1 % Trifluoroacetic acid through vortexing and sonication. The homogeneous solution of peptide was kept for 11-15 days at ambient temperature (~2-8 °C) to form assembly formation.

Circular Dichroism

A JASCO J-810 circular dichroism spectrometer fitted with a Peltier temperature controller to maintain the temperature at 25 °C was used to record the CD spectra. 200 μM of Ac-KE (stock 2.5 mM) aged assemblies was taken in Mili-Q water and the spectra were recorded in a quartz cuvette with a 1 mm path length. Spectrum was recorded throughout the wavelength range from 300 nm to 180 nm with a scan rate of 100 nm/min and two accumulations.

Thioflavin T assay

The 11-15 days matured assembly Ac-KE peptide (300 μM) was mixed with different concentrations of ATP (6 and 20 mM) in 10 mM of HEPES buffer (pH 7.2) at room temperature. 30 μM of ThT dye was added to the mixture and started the experiment with excitation wavelength (λ_{ex}) at 440 nm and emission (λ_{em}) at 480 nm. Kinetics was recorded for 18 h with 30 min intervals, and 30 sec constant shaking was set before taking the data. The gain was fixed to 50 in the microplate reader (BioTek, SYNERGY H1). To check the control, only Ac-KE (300 μM) was taken in a similar environment and data were recorded.

To check ThT as a reporter for amyloid assembly fluorescence spectra in microplate reader was checked for 200 μM of Ac-KE assembly in presence of 30 μM ThT. The excitation wavelength and gain were set at 440 nm and 50 respectively.

Acknowledgement

We acknowledge support of the Department of Atomic Energy, Government of India, under Project Identification No. RTI 4007. JM thanks Core Research grants provided by the Department of Science and Technology (DST) of India (CRG/2023/001426).

References:

(1) Patel, A.; Malinovska, L.; Saha, S.; Wang, J.; Alberti, S.; Krishnan, Y.; Hyman, A. A. ATP as a Biological Hydrotrope. *Science* **2017**, *356* (6339), 753–756.
(2) Sridharan, S.; Kurzawa, N.; Werner, T.; Günthner, I.; Helm, D.; Huber, W.; Bantscheff, M.; Savitski, M. M. Proteome-Wide Solubility and Thermal Stability Profiling Reveals Distinct Regulatory Roles for ATP. *Nat. Commun.* **2019**, *10* (1), 1155.
(3) Nishizawa, M.; Walinda, E.; Morimoto, D.; Kohn, B.; Scheler, U.; Shirakawa, M.; Sugase, K. Effects of Weak Nonspecific Interactions with ATP on Proteins. *J. Am. Chem. Soc.* **2021**, *143* (31), 11982–11993.
(4) Kim, T. H.; Payliss, B. J.; Nosella, M. L.; Lee, I. T. W.; Toyama, Y.; Forman-Kay, J. D.; Kay, L. E. Interaction Hot Spots for Phase Separation Revealed by NMR Studies of a CAPRIN1 Condensed Phase. *Proc. Natl. Acad. Sci. U. S. A.* **2021**, *118* (23). https://doi.org/10.1073/pnas.2104897118.
(5) Sridharan, S.; Kurzawa, N.; Werner, T.; Günthner, I.; Helm, D.; Huber, W.; Bantscheff, M.; Savitski, M. M. Proteome-Wide Solubility and Thermal Stability Profiling Reveals Distinct Regulatory Roles for ATP. *Nat. Commun.* **2019**, *10* (1), 1155.
(6) Ou, X.; Lao, Y.; Xu, J.; Wutthinitikornkit, Y.; Shi, R.; Chen, X.; Li, J. ATP Can Efficiently Stabilize Protein through a Unique Mechanism. *JACS Au* **2021**, *1* (10), 1766–1777.
(7) Song, J. Adenosine Triphosphate Energy-Independently Controls Protein Homeostasis with Unique Structure and Diverse Mechanisms. *Protein Sci.* **2021**, *30* (7), 1277–1293.
(8) Sridharan, S.; Kurzawa, N.; Werner, T.; Günthner, I.; Helm, D.; Huber, W.; Bantscheff, M.; Savitski, M. M. Proteome-Wide Solubility and Thermal Stability Profiling Reveals Distinct Regulatory Roles for ATP. *Nat. Commun.* **2019**, *10* (1), 1155.
(9) Patel, A.; Malinovska, L.; Saha, S.; Wang, J.; Alberti, S.; Krishnan, Y.; Hyman, A. A. ATP as a Biological Hydrotrope. *Science* **2017**, *356* (6339), 753–756.
(10) He, Y.; Kang, J.; Song, J. ATP Antagonizes the Crowding-Induced Destabilization of the Human Eye-

Lens Protein γS-Crystallin. *Biochem. Biophys. Res. Commun.* **2020**, *526* (4), 1112–1117.
(11) Aida, H.; Shigeta, Y.; Harada, R. The Role of ATP in Solubilizing RNA-Binding Protein Fused in Sarcoma. *Proteins* **2022**, *90* (8), 1606–1612.
(12) Pal, S.; Paul, S. ATP Controls the Aggregation of Aβ Peptides. *J. Phys. Chem. B* **2020**, *124* (1), 210–223.
(13) Sarkar, S.; Mondal, J. Mechanistic Insights on ATP's Role as a Hydrotrope. *J. Phys. Chem. B* **2021**, *125* (28), 7717–7731.
(14) Patel, A.; Malinovska, L.; Saha, S.; Wang, J.; Alberti, S.; Krishnan, Y.; Hyman, A. A. ATP as a Biological Hydrotrope. *Science* **2017**, *356* (6339), 753–756.
(15) Pal, S.; Paul, S. ATP Controls the Aggregation of Aβ Peptides. *J. Phys. Chem. B* **2020**, *124* (1), 210–223.
(16) He, Y.; Kang, J.; Song, J. ATP Antagonizes the Crowding-Induced Destabilization of the Human Eye-Lens Protein γS-Crystallin. *Biochem. Biophys. Res. Commun.* **2020**, *526* (4), 1112–1117.
(17) Sarkar, S.; Narayanan, T. N.; Mondal, J. A Synergistic View on Osmolyte's Role against Salt and Cold Stress in Biointerfaces. *Langmuir* **2023**, *39* (49), 17581–17592.
(18) Hayes, M. H.; Peuchen, E. H.; Dovichi, N. J.; Weeks, D. L. Dual Roles for ATP in the Regulation of Phase Separated Protein Aggregates in Oocyte Nucleoli. *Elife* **2018**, *7*. https://doi.org/10.7554/eLife.35224.
(19) Sarkar, S.; Guha, A.; Narayanan, T. N.; Mondal, J. Zwitterionic Osmolytes Revive Surface Charges under Salt Stress via Dual Mechanisms. *J. Phys. Chem. Lett.* **2022**, *13* (24), 5660–5668.
(20) Sarkar, S.; Guha, A.; Sadhukhan, R.; Narayanan, T. N.; Mondal, J. Osmolytes as Cryoprotectants under Salt Stress. *ACS Biomater Sci Eng* **2023**, *9* (10), 5639–5652.
(21) Greiner, J. V.; Glonek, T. Intracellular ATP Concentration and Implication for Cellular Evolution. *Biology* **2021**, *10* (11). https://doi.org/10.3390/biology10111166.
(22) Robustelli, P.; Piana, S.; Shaw, D. E. Developing a Molecular Dynamics Force Field for Both Folded and Disordered Protein States. *Proc. Natl. Acad. Sci. U. S. A.* **2018**, *115* (21), E4758–E4766.
(23) Jana, A. K.; Batkulwar, K. B.; Kulkarni, M. J.; Sengupta, N. Glycation Induces Conformational Changes in the Amyloid-β Peptide and Enhances Its Aggregation Propensity: Molecular Insights. *Phys. Chem. Chem. Phys.* **2016**, *18* (46), 31446–31458.
(24) Sridharan, S.; Kurzawa, N.; Werner, T.; Günthner, I.; Helm, D.; Huber, W.; Bantscheff, M.; Savitski, M. M. Proteome-Wide Solubility and Thermal Stability Profiling Reveals Distinct Regulatory Roles for ATP. *Nat. Commun.* **2019**, *10* (1), 1155.
(25) Tarus, B.; Straub, J. E.; Thirumalai, D. Dynamics of Asp23-Lys28 Salt-Bridge Formation in Abeta10-35 Monomers. *J. Am. Chem. Soc.* **2006**, *128* (50), 16159–16168.
(26) Sgourakis, N. G.; Yan, Y.; McCallum, S. A.; Wang, C.; Garcia, A. E. The Alzheimer's Peptides Abeta40 and 42 Adopt Distinct Conformations in Water: A Combined MD / NMR Study. *J. Mol. Biol.* **2007**, *368* (5), 1448–1457.
(27) Larini, L.; Shea, J.-E. Role of β-Hairpin Formation in Aggregation: The Self-Assembly of the Amyloid-β(25-35) Peptide. *Biophys. J.* **2012**, *103* (3), 576–586.
(28) Sridharan, S.; Kurzawa, N.; Werner, T.; Günthner, I.; Helm, D.; Huber, W.; Bantscheff, M.; Savitski, M. M. Proteome-Wide Solubility and Thermal Stability Profiling Reveals Distinct Regulatory Roles for ATP. *Nat. Commun.* **2019**, *10* (1), 1155.
(29) Tarus, B.; Straub, J. E.; Thirumalai, D. Dynamics of Asp23-Lys28 Salt-Bridge Formation in Abeta10-35 Monomers. *J. Am. Chem. Soc.* **2006**, *128* (50), 16159–16168.
(30) Sridharan, S.; Kurzawa, N.; Werner, T.; Günthner, I.; Helm, D.; Huber, W.; Bantscheff, M.; Savitski, M. M. Proteome-Wide Solubility and Thermal Stability Profiling Reveals Distinct Regulatory Roles for ATP. *Nat. Commun.* **2019**, *10* (1), 1155.
(31) Tarus, B.; Straub, J. E.; Thirumalai, D. Dynamics of Asp23-Lys28 Salt-Bridge Formation in Abeta10-35 Monomers. *J. Am. Chem. Soc.* **2006**, *128* (50), 16159–16168.
(32) Sridharan, S.; Kurzawa, N.; Werner, T.; Günthner, I.; Helm, D.; Huber, W.; Bantscheff, M.; Savitski, M. M. Proteome-Wide Solubility and Thermal Stability Profiling Reveals Distinct Regulatory Roles for ATP. *Nat. Commun.* **2019**, *10* (1), 1155.
(33) Tarus, B.; Straub, J. E.; Thirumalai, D. Dynamics of Asp23-Lys28 Salt-Bridge Formation in Abeta10-35 Monomers. *J. Am. Chem. Soc.* **2006**, *128* (50), 16159–16168.
(34) Mehta, A. K.; Lu, K.; Childers, W. S.; Liang, Y.; Dublin, S. N.; Dong, J.; Snyder, J. P.; Pingali, S. V.; Thiyagarajan, P.; Lynn, D. G. Facial Symmetry in Protein Self-Assembly. *J. Am. Chem. Soc.* **2008**, *130* (30), 9829–9835.

(35) Hsieh, M.-C.; Lynn, D. G.; Grover, M. A. Kinetic Model for Two-Step Nucleation of Peptide Assembly. *J. Phys. Chem. B* **2017**, *121* (31), 7401–7411.
(36) Harada, T.; Kuroda, R. CD Measurements of β-Amyloid (1-40) and (1-42) in the Condensed Phase. *Biopolymers* **2011**, *95* (2), 127–134.
(37) Sulatskaya, A. I.; Kuznetsova, I. M.; Turoverov, K. K. Interaction of Thioflavin T with Amyloid Fibrils: Stoichiometry and Affinity of Dye Binding, Absorption Spectra of Bound Dye. *J. Phys. Chem. B* **2011**, *115* (39), 11519–11524.
(38) Biancalana, M.; Makabe, K.; Koide, A.; Koide, S. Molecular Mechanism of Thioflavin-T Binding to the Surface of Beta-Rich Peptide Self-Assemblies. *J. Mol. Biol.* **2009**, *385* (4), 1052–1063.
(39) Fatafta, H.; Khaled, M.; Owen, M. C.; Sayyed-Ahmad, A.; Strodel, B. Amyloid-β Peptide Dimers Undergo a Random Coil to β-Sheet Transition in the Aqueous Phase but Not at the Neuronal Membrane. *Proc. Natl. Acad. Sci. U. S. A.* **2021**, *118* (39). https://doi.org/10.1073/pnas.2106210118.
(40) Zheng, J.; Jang, H.; Ma, B.; Tsai, C.-J.; Nussinov, R. Modeling the Alzheimer Abeta17-42 Fibril Architecture: Tight Intermolecular Sheet-Sheet Association and Intramolecular Hydrated Cavities. *Biophys. J.* **2007**, *93* (9), 3046–3057.
(41) Nishizawa, M.; Walinda, E.; Morimoto, D.; Kohn, B.; Scheler, U.; Shirakawa, M.; Sugase, K. Effects of Weak Nonspecific Interactions with ATP on Proteins. *J. Am. Chem. Soc.* **2021**, *143* (31), 11982–11993.
(42) Zalar, M.; Bye, J.; Curtis, R. Nonspecific Binding of Adenosine Tripolyphosphate and Tripolyphosphate Modulates the Phase Behavior of Lysozyme. *J. Am. Chem. Soc.* **2023**, *145* (2), 929–943.
(43) Song, J. Adenosine Triphosphate Energy-Independently Controls Protein Homeostasis with Unique Structure and Diverse Mechanisms. *Protein Sci.* **2021**, *30* (7), 1277–1293.
(44) Kim, T. H.; Payliss, B. J.; Nosella, M. L.; Lee, I. T. W.; Toyama, Y.; Forman-Kay, J. D.; Kay, L. E. Interaction Hot Spots for Phase Separation Revealed by NMR Studies of a CAPRIN1 Condensed Phase. *Proc. Natl. Acad. Sci. U. S. A.* **2021**, *118* (23). https://doi.org/10.1073/pnas.2104897118.
(45) Sridharan, S.; Kurzawa, N.; Werner, T.; Günthner, I.; Helm, D.; Huber, W.; Bantscheff, M.; Savitski, M. M. Proteome-Wide Solubility and Thermal Stability Profiling Reveals Distinct Regulatory Roles for ATP. *Nat. Commun.* **2019**, *10* (1), 1155.
(46) Pal, S.; Paul, S. ATP Controls the Aggregation of Aβ Peptides. *J. Phys. Chem. B* **2020**, *124* (1), 210–223.
(47) Sarkar, S.; Mondal, J. Mechanistic Insights on ATP's Role as a Hydrotrope. *J. Phys. Chem. B* **2021**, *125* (28), 7717–7731.
(48) Dec, R.; Jaworek, M. W.; Dzwolak, W.; Winter, R. Liquid-Droplet-Mediated ATP-Triggered Amyloidogenic Pathway of Insulin-Derived Chimeric Peptides: Unraveling the Microscopic and Molecular Processes. *J. Am. Chem. Soc.* **2023**. https://doi.org/10.1021/jacs.2c12611.
(49) Sridharan, S.; Kurzawa, N.; Werner, T.; Günthner, I.; Helm, D.; Huber, W.; Bantscheff, M.; Savitski, M. M. Proteome-Wide Solubility and Thermal Stability Profiling Reveals Distinct Regulatory Roles for ATP. *Nat. Commun.* **2019**, *10* (1), 1155.
(50) Ren, C.-L.; Shan, Y.; Zhang, P.; Ding, H.-M.; Ma, Y.-Q. Uncovering the Molecular Mechanism for Dual Effect of ATP on Phase Separation in FUS Solution. *Sci Adv* **2022**, *8* (37), eabo7885.
(51) Song, J. Adenosine Triphosphate Energy-Independently Controls Protein Homeostasis with Unique Structure and Diverse Mechanisms. *Protein Sci.* **2021**, *30* (7), 1277–1293.
(52) Liu, F.; Wang, J. ATP Acts as a Hydrotrope to Regulate the Phase Separation of NBDY Clusters. *JACS Au* **2023**, *3* (9), 2578–2585.
(53) Sridharan, S.; Kurzawa, N.; Werner, T.; Günthner, I.; Helm, D.; Huber, W.; Bantscheff, M.; Savitski, M. M. Proteome-Wide Solubility and Thermal Stability Profiling Reveals Distinct Regulatory Roles for ATP. *Nat. Commun.* **2019**, *10* (1), 1155.
(54) Saraste, M.; Sibbald, P. R.; Wittinghofer, A. The P-Loop--a Common Motif in ATP- and GTP-Binding Proteins. *Trends Biochem. Sci.* **1990**, *15* (11), 430–434.
(55) Robustelli, P.; Piana, S.; Shaw, D. E. Developing a Molecular Dynamics Force Field for Both Folded and Disordered Protein States. *Proc. Natl. Acad. Sci. U. S. A.* **2018**, *115* (21), E4758–E4766.
(56) Nosé, S. A Molecular Dynamics Method for Simulations in the Canonical Ensemble. *Mol. Phys.* **1984**, *52* (2), 255–268.
(57) Hoover, W. G. Canonical Dynamics: Equilibrium Phase-Space Distributions. *Phys. Rev. A Gen. Phys.* **1985**, *31* (3), 1695–1697.
(58) Berendsen, H. J. C.; Grigera, J. R.; Straatsma, T. P. The Missing Term in Effective Pair Potentials. *J. Phys. Chem.* **1987**, *91* (24), 6269–6271.

(59) Parrinello, M.; Rahman, A. Polymorphic Transitions in Single Crystals: A New Molecular Dynamics Method. *J. Appl. Phys.* **1981**, *52* (12), 7182–7190.
(60) Parrinello, M.; Rahman, A. Polymorphic Transitions in Single Crystals: A New Molecular Dynamics Method. *J. Appl. Phys.* **1981**, *52* (12), 7182–7190.
(61) Darden, T.; York, D.; Pedersen, L. Particle Mesh Ewald: An $N \cdot \log(N)$ Method for Ewald Sums in Large Systems. *J. Chem. Phys.* **1993**, *98* (12), 10089–10092.
(62) Hess, B. P-LINCS: A Parallel Linear Constraint Solver for Molecular Simulation. *J. Chem. Theory Comput.* **2008**, *4* (1), 116–122.
(63) Hess, B. P-LINCS: A Parallel Linear Constraint Solver for Molecular Simulation. *J. Chem. Theory Comput.* **2008**, *4* (1), 116–122.
(64) Miyamoto, S.; Kollman, P. A. Settle: An Analytical Version of the SHAKE and RATTLE Algorithm for Rigid Water Models. *J. Comput. Chem.* **1992**, *13* (8), 952–962.
(65) Abraham, M. J.; Murtola, T.; Schulz, R.; Páll, S.; Smith, J. C.; Hess, B.; Lindahl, E. GROMACS: High Performance Molecular Simulations through Multi-Level Parallelism from Laptops to Supercomputers. *SoftwareX* **2015**, *1-2*, 19–25.
(66) Sugita, Y.; Okamoto, Y. Replica-Exchange Molecular Dynamics Method for Protein Folding. *Chem. Phys. Lett.* **1999**, *314* (1-2), 141–151.
(67) Best, R. B.; Zhu, X.; Shim, J.; Lopes, P. E. M.; Mittal, J.; Feig, M.; Mackerell, A. D., Jr. Optimization of the Additive CHARMM All-Atom Protein Force Field Targeting Improved Sampling of the Backbone φ, ψ and Side-Chain χ(1) and χ(2) Dihedral Angles. *J. Chem. Theory Comput.* **2012**, *8* (9), 3257–3273.
(68) Best, R. B.; Zhu, X.; Shim, J.; Lopes, P. E. M.; Mittal, J.; Feig, M.; Mackerell, A. D., Jr. Optimization of the Additive CHARMM All-Atom Protein Force Field Targeting Improved Sampling of the Backbone φ, ψ and Side-Chain χ(1) and χ(2) Dihedral Angles. *J. Chem. Theory Comput.* **2012**, *8* (9), 3257–3273.
(69) Sarkar, S.; Mondal, J. Mechanistic Insights on ATP's Role as a Hydrotrope. *J. Phys. Chem. B* **2021**, *125* (28), 7717–7731.
(70) MacKerell, A. D.; Bashford, D.; Bellott, M.; Dunbrack, R. L.; Evanseck, J. D.; Field, M. J.; Fischer, S.; Gao, J.; Guo, H.; Ha, S.; Joseph-McCarthy, D.; Kuchnir, L.; Kuczera, K.; Lau, F. T.; Mattos, C.; Michnick, S.; Ngo, T.; Nguyen, D. T.; Prodhom, B.; Reiher, W. E.; Roux, B.; Schlenkrich, M.; Smith, J. C.; Stote, R.; Straub, J.; Watanabe, M.; Wiórkiewicz-Kuczera, J.; Yin, D.; Karplus, M. All-Atom Empirical Potential for Molecular Modeling and Dynamics Studies of Proteins. *J. Phys. Chem. B* **1998**, *102* (18), 3586–3616.
(71) Robustelli, P.; Piana, S.; Shaw, D. E. Developing a Molecular Dynamics Force Field for Both Folded and Disordered Protein States. *Proc. Natl. Acad. Sci. U. S. A.* **2018**, *115* (21), E4758–E4766.
(72) Robustelli, P.; Piana, S.; Shaw, D. E. Developing a Molecular Dynamics Force Field for Both Folded and Disordered Protein States. *Proc. Natl. Acad. Sci. U. S. A.* **2018**, *115* (21), E4758–E4766.
(73) Sarkar, S.; Mondal, J. Mechanistic Insights on ATP's Role as a Hydrotrope. *J. Phys. Chem. B* **2021**, *125* (28), 7717–7731.
(74) MacKerell, A. D.; Bashford, D.; Bellott, M.; Dunbrack, R. L.; Evanseck, J. D.; Field, M. J.; Fischer, S.; Gao, J.; Guo, H.; Ha, S.; Joseph-McCarthy, D.; Kuchnir, L.; Kuczera, K.; Lau, F. T.; Mattos, C.; Michnick, S.; Ngo, T.; Nguyen, D. T.; Prodhom, B.; Reiher, W. E.; Roux, B.; Schlenkrich, M.; Smith, J. C.; Stote, R.; Straub, J.; Watanabe, M.; Wiórkiewicz-Kuczera, J.; Yin, D.; Karplus, M. All-Atom Empirical Potential for Molecular Modeling and Dynamics Studies of Proteins. *J. Phys. Chem. B* **1998**, *102* (18), 3586–3616.
(75) Hart, K.; Foloppe, N.; Baker, C. M.; Denning, E. J.; Nilsson, L.; Mackerell, A. D., Jr. Optimization of the CHARMM Additive Force Field for DNA: Improved Treatment of the BI/BII Conformational Equilibrium. *J. Chem. Theory Comput.* **2012**, *8* (1), 348–362.
(76) Husic, B. E.; Pande, V. S. Markov State Models: From an Art to a Science. *J. Am. Chem. Soc.* **2018**, *140* (7), 2386–2396.
(77) Husic, B. E.; Pande, V. S. Markov State Models: From an Art to a Science. *J. Am. Chem. Soc.* **2018**, *140* (7), 2386–2396.
(78) Scherer, M. K.; Trendelkamp-Schroer, B.; Paul, F.; Pérez-Hernández, G.; Hoffmann, M.; Plattner, N.; Wehmeyer, C.; Prinz, J.-H.; Noé, F. PyEMMA 2: A Software Package for Estimation, Validation, and Analysis of Markov Models. *J. Chem. Theory Comput.* **2015**, *11* (11), 5525–5542.
(79) Tribello, G. A.; Bonomi, M.; Branduardi, D.; Camilloni, C.; Bussi, G. PLUMED 2: New Feathers for an Old Bird. *Comput. Phys. Commun.* **2014**, *185* (2), 604–613.

(80) Gowers, R.; Linke, M.; Barnoud, J.; Reddy, T.; Melo, M.; Seyler, S.; Domański, J.; Dotson, D.; Buchoux, S.; Kenney, I.; Beckstein, O. MDAnalysis: A Python Package for the Rapid Analysis of Molecular Dynamics Simulations. In *Proceedings of the 15th Python in Science Conference*; SciPy, 2016. https://doi.org/10.25080/majora-629e541a-00e.
(81) Wyman, J., Jr. LINKED FUNCTIONS AND RECIPROCAL EFFECTS IN HEMOGLOBIN: A SECOND LOOK. *Adv. Protein Chem.* **1964**, *19*, 223–286.
(82) Tanford, C. Extension of the Theory of Linked Functions to Incorporate the Effects of Protein Hydration. *J. Mol. Biol.* **1969**, *39* (3), 539–544.